

# DCP-Prune: Ultra-Low Token Pruning with Distribution Consistency Preservation

Xifeng Xue<sup>1</sup>, Xiaokang Wang<sup>2</sup>, Zirui Li<sup>1</sup>, Ming-Ming Cheng<sup>1</sup>, Guolei Sun<sup>1\*</sup>

<sup>1</sup>College of Computer Science, Nankai University, Tianjin, China

<sup>2</sup>Nanjing University of Posts and Telecommunications, Nanjing, China

## Abstract

Recent vision token pruning methods effectively preserve model performance under moderate token budgets but become unstable under ultra-low token budget. Our analysis shows that as the pruning budget decreases, accuracy degradation is often accompanied by larger feature distribution shifts. Critically, the degree of this distribution shift strongly correlates with performance degradation. To better characterize this phenomenon, we introduce a lightweight distribution consistency metric to estimate the distribution shift between retained and full tokens. Motivated by these observations, we propose a two-stage pruning framework consisting of Anchor-Context Graph Recovery (ACGR) and Text-Aware Token Cluster Selection (TATCS). Specifically, ACGR transfers contextual information before token removal, while TATCS dynamically re-selects representative tokens when severe distribution shift is detected. Extensive experiments demonstrate that our method achieves superior and more stable performance under ultra-low token budget. Notably, it retains 92.1% of the upper-bound average performance on LLaVA-1.5-7B with only 16 visual tokens. The code will be released at: <https://github.com/EMVision-NK/DCP-Prune>.

## 1 Introduction

Vision-language models (VLMs) have recently demonstrated strong performance across a broad range of multimodal tasks, including visual question answering (Dai et al., 2023; Alayrac et al., 2022; Huang et al., 2023; Li et al., 2023a), image understanding (Zhu et al., 2024; Liu et al., 2023; Chen et al., 2022, 2024b), and multimodal dialogue (Li et al., 2024c; Wang et al., 2024b; Li et al., 2024a; Wang et al., 2024c). However, the computational cost of VLMs grows rapidly with increasingly complex visual inputs. In VLMs, the number

of visual tokens scales rapidly with higher image resolutions (Guo et al., 2024; Deghani et al., 2023; Dong et al., 2024), multi-image inputs (Wang et al., 2023; Ye et al., 2023; Moon et al., 2024; Chen et al., 2023), and video sequences (Li et al., 2024b; Arnab et al., 2021; Bain et al., 2021; Sun et al., 2019). As a result, memory usage and inference latency increase substantially, posing a significant obstacle to practical deployment and making visual token pruning a critical research problem.

Existing visual token pruning methods are generally categorized into importance-oriented methods and coverage-oriented methods, and both have shown strong performance under moderate token budgets (Jiang et al., 2025; Zhang et al., 2025c; Tan et al., 2025; Zhang et al., 2025a). However, their performance often becomes unsatisfactory under *ultra-low* token budgets. Specifically, importance-oriented methods preserve salient tokens, but often suffer from redundancy and loss of contextual information under aggressive compression (Shang et al., 2025; Sun et al., 2025; Yang et al., 2025b; Li et al., 2025b). In contrast, coverage-oriented methods prioritize spatial or semantic diversity, but may retain tokens that are less informative for reasoning (Kim et al., 2025; Chen et al., 2025; Zhang et al., 2025b; Yu et al., 2026). Consequently, under ultra-low token budget, both strategies progressively drive retained tokens away from the original feature distribution, degrading performance.

The distribution shift between retained and full tokens leads to performance degradation under ultra-low token budget (Zhang et al., 2026; Duan et al., 2022). To better characterize this phenomenon, we introduce a lightweight distribution consistency metric:

$$\mathcal{D}(X_k, X_f) = \frac{\text{Tr}(\Sigma_k) + d \text{Var}(\mu_k)}{\text{Tr}(\Sigma_f) + d \text{Var}(\mu_f)}, \quad (1)$$
$$\kappa = |\mathcal{D}(X_k, X_f) - 1|,$$

where  $X_f$  and  $X_k$  denote the full and kept token

\*Corresponding author.

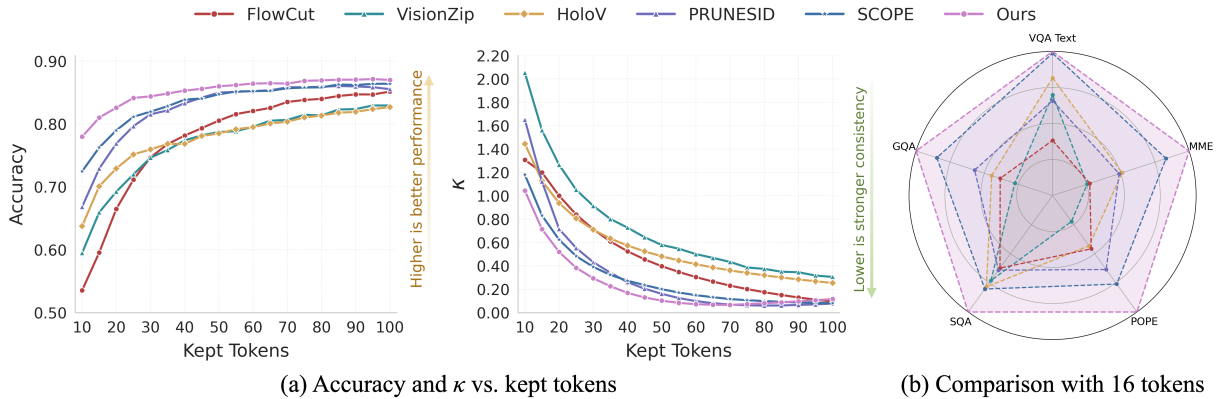


Figure 1: (a) Relationship between kept tokens, distribution deviation ( $\kappa$ ), and accuracy for LLaVA-1.5-7B on POPE dataset. (b) Performance comparison under the ultra-low budget of 16 retained tokens.

sets, respectively.  $\text{Tr}(\Sigma)$  measures feature dispersion, while  $\text{Var}(\mu)$  reflects shifts in channel-wise feature statistics. Using this metric, Fig. 1(a) shows that reducing the token budget consistently enlarges the distributional discrepancy between retained and full tokens, accompanied by severe performance degradation. This aligned trend suggests that distributional discrepancy serves as an informative indicator of pruning regimes prone to performance degradation.

Motivated by the relation between distributional discrepancy and performance degradation, we design a two-stage framework for ultra-low visual token pruning. During progressive pruning, **Anchor-Context Graph Recovery (ACGR)** transfers contextual information from tokens to be discarded into retained tokens, thereby alleviating loss of semantic information and maintaining token distribution under aggressive pruning. At the final pruning stage, **Text-Aware Token Cluster Selection (TATCS)** is triggered under significant feature distribution shifts to reselect representative tokens with textual guidance, helping retain task-relevant visual information while improving feature distribution consistency. As illustrated in Fig. 1(b), our framework achieves much better performance under ultra-low token budget, compared with existing methods. Our contributions are threefold:

(1) We observe that ultra-low token pruning induces distribution shift between retained and full tokens, and further introduce a lightweight metric to quantify this shift, showing that the discrepancy closely aligns with performance degradation.

(2) We propose a two-stage pruning framework consisting of Anchor-Context Graph Recovery (ACGR) and Text-Aware Token Cluster Selection (TATCS) to respectively mitigate contextual infor-

mation loss and distribution shift under ultra-low token budget.

(3) Extensive experiments on various VLMs demonstrate that our method consistently outperforms existing pruning methods under ultra-low token budget, retaining 92.1% performance on LLaVA-1.5-7B with 16 tokens under (97.2% reduction) and 91.9% performance on LLaVA-NeXT-7B with 80 tokens under (97.2% reduction).

## 2 Related Works

**Visual Token Pruning in VLMs.** Visual token pruning has emerged as an effective strategy for improving VLMs efficiency by removing redundant visual tokens during inference. Early studies show that many visual tokens contribute little to predictions and can be safely pruned based on attention or feature responses (Chen et al., 2024a). Subsequent work improves token selection by incorporating information flow or transformation dynamics, such as (Tong et al., 2025). Other approaches attempt to balance token importance and diversity (Deng et al., 2025) or explicitly model redundancy and diversity in token selection (Fang et al., 2026). Despite these advances, most methods select tokens by importance or coverage, largely overlooking distributional consistency. Under ultra-low token budgets, retained tokens can deviate from the original feature distribution, making it harder to preserve a compact yet representative subset.

**Distribution Consistency in Token Pruning.** Under ultra-low token pruning, retained visual token distributions progressively deviate from the original full token distribution. Recent studies on visual token pruning show that aggressive compression introduces selection bias and weakens

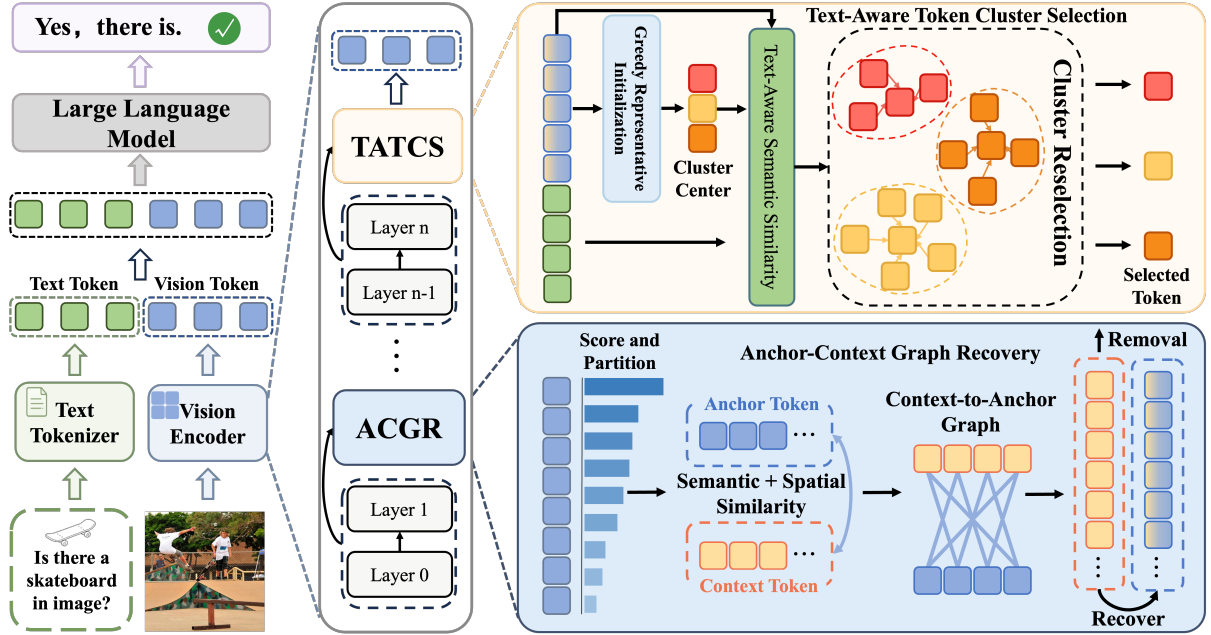


Figure 2: Overview of the proposed two-stage ultra-low token pruning framework. ACGR transfers contextual information from pruned context tokens to retained anchor tokens to alleviate semantic loss. TATCS mitigates distribution drift by reselecting representative tokens using text-aware semantic similarity.

fine-grained visual understanding (Endo et al., 2025). More broadly, distribution modeling has been widely used to characterize representation discrepancy. For example, (Liang et al., 2025) models semantic features with Gaussian distributions for feature alignment, while (Zhang et al., 2023) theoretically analyzes divergence measures between Gaussian feature distributions. These studies suggest that feature distributions can be characterized through their statistical properties, providing a way to assess representation mismatch. In contrast, most existing visual token pruning methods focus on token importance or diversity, without explicitly considering whether the retained subset preserves the original statistical structure. Under aggressive pruning, this mismatch becomes more pronounced, making the retained tokens less representative and degrading multimodal reasoning performance.

### 3 Method

#### 3.1 Overview

Given a set of  $d$ -dimensional visual tokens  $X_f \in \mathbb{R}^{N \times d}$ , our objective is to select a compact kept subset  $X_k \in \mathbb{R}^{K \times d}$  under an ultra-low token budget ( $K \ll N$ ). During progressive pruning, the retained tokens should preserve task-relevant visual semantics while retaining complementary contextual information. Meanwhile, the kept tokens representations should remain consistent with the original full token distribution under ultra-low to-

ken budget.

In this paper, we propose a two-stage pruning framework, illustrated in Fig. 2. During progressive pruning, ACGR is employed to aggregate contextual information from discarded tokens into retained anchor tokens prior to token removal, thereby preserving richer visual semantics under aggressive compression. At the final pruning stage, where severe distribution shift may arise, TATCS is introduced to perform text-aware representative token reselection from the original token pool, helping maintain feature distribution consistency under ultra-low token budget.

#### 3.2 Anchor-Context Graph Recovery

Under ultra-low token budget, directly discarding visual tokens inevitably removes complementary semantic and spatial information. As pruning intensifies, the contextual relationships among tokens are increasingly disrupted, making the remaining tokens less representative of the original visual semantics. To address this issue, we propose Anchor-Context Graph Recovery (ACGR), which transfers contextual information from discarded contextual tokens to retained anchor tokens before pruning, thereby preserving richer visual semantics under aggressive pruning.

Given the token set  $X = \{x_i\}_{i=1}^M$  at the current pruning stage, we first perform *score and partition* by computing an overall importance score for each

token as:

$$s_i = s_i^{\text{cls}} + s_i^{\text{cos}} + s_i^{\text{var}} + s_i^{\text{abl}}. \quad (2)$$

Here,  $s_i^{\text{cls}}$ ,  $s_i^{\text{cos}}$ ,  $s_i^{\text{var}}$ , and  $s_i^{\text{abl}}$  measure CLS relevance, feature non-redundancy, transformation variation, and attention-ablation impact, respectively. These criteria jointly capture global semantic importance, redundancy suppression, feature dynamics, and token influence through attention interactions. Detailed formulations and normalization strategies are provided in Appendix A. Based on the resulting scores  $s_i$ , the token set  $X$  is then partitioned into an anchor set  $X_a = \{x_j^a\}_{j=1}^{M_a}$  and a context set  $X_c = \{x_i^c\}_{i=1}^{M_c}$ , where  $M_a$  and  $M_c$  denote the numbers of retained anchor tokens and discarded context tokens, respectively.

Instead of directly discarding context tokens, ACGR constructs a semantic-spatial context-to-anchor graph to transfer complementary information from  $X_c$  to  $X_a$ . Since semantically similar and spatially nearby tokens are more likely to provide complementary information, we measure token affinity using both *semantic and spatial similarity*. Accordingly, the edge weight between context token  $x_i^c$  and anchor token  $x_j^a$  is defined as

$$e_{ij} = \cos(x_i^c, x_j^a) \cdot \exp\left(-\frac{\|p_i^c - p_j^a\|_2^2}{\tau}\right). \quad (3)$$

where  $p_i^c$  and  $p_j^a$  denote token grid coordinates, and  $\tau$  controls spatial decay. To suppress noisy information transfer, each anchor token retains only its top- $k_n$  context neighbors. Finally, the retained anchor tokens are updated through residual aggregation over the *context-to-anchor graph*:

$$\tilde{x}_j^a = x_j^a + \alpha \sum_{i \in \mathcal{N}_{k_n}(j)} \bar{e}_{ij} x_i^c, \quad (4)$$

where  $\bar{e}_{ij} = e_{ij} / \sum_{i \in \mathcal{N}_{k_n}(j)} e_{ij}$  denotes the normalized edge weight,  $\mathcal{N}_{k_n}(j)$  denotes the top- $k_n$  neighbors of  $x_j^a$ , and  $\alpha$  is the fusion coefficient.

The recovered anchor set  $\tilde{X}_a = \{\tilde{x}_j^a\}_{j=1}^{M_a}$  maintains the same token budget as direct pruning while incorporating complementary semantic-spatial information from discarded tokens. As a result, ACGR mitigates the representation degradation caused by progressive pruning under aggressive compression.

### 3.3 Text-Aware Token Cluster Selection

Although ACGR alleviates contextual information loss during progressive pruning, the retained token

subset can still gradually drift from the original feature distribution under ultra-low token budget, reducing the representativeness of the kept tokens. To address this, TATCS is activated at the final pruning stage when significant distribution shift is detected, performing text-aware token reselection from  $X$  to restore distributional consistency.

At the final pruning stage, we first compute the distribution consistency metric  $\kappa$  using Eq. 1 between the retained anchor tokens  $X_a$  and the input token set  $X$ . When  $\kappa > \delta$ , where  $\delta$  is a predefined instability threshold, the retained subset is considered to exhibit severe distribution drift and becomes less representative of the original visual semantics. Under this condition, TATCS is applied at the final pruning stage to perform text-aware token reselection and restore feature distribution consistency. A statistical interpretation of  $\kappa$  is provided in Appendix B.

Then, under the target token budget  $K$ , we perform *greedy representative initialization* on  $X$  to obtain a representative token subset. Specifically, during each greedy selection step, every candidate token  $x_i \in U$  is evaluated by

$$G_i = \frac{1}{|U|} \sum_{x_j \in U} \cos(x_i, x_j) - \max_{x_p \in S} \cos(x_i, x_p) + \hat{a}_i^{\text{cls}}, \quad (5)$$

where  $S$  and  $U$  denote the selected token set and the unselected candidate token set, respectively, with  $U = X$  at initialization, and  $\hat{a}_i^{\text{cls}}$  is the normalized CLS attention score. At each iteration, the token with the largest gain  $G_i$  is added to  $S$ . The process is repeated until  $K$  representative tokens are selected, and the selected token set  $S = \{z_k\}_{k=1}^K$  is used as the initial cluster centers.

Given the text feature  $t$  extracted from the input text, we define a *text-aware semantic similarity* between token  $x_i$  and cluster center  $z_k$  by jointly modeling their visual similarity and text-alignment consistency:

$$\text{sim}_{ik} = \cos(x_i, z_k) - |\cos(x_i, t) - \cos(z_k, t)|, \quad (6)$$

where the first term captures visual similarity, while the second term enforces consistency in text relevance between tokens assigned to the same cluster. Based on this similarity, each token is assigned through text-aware assignment:

$$c_i = \arg \max_k \text{sim}_{ik}. \quad (7)$$

The cluster centers are then iteratively updated

by averaging the assigned token features:

$$\tilde{z}_k = \frac{\sum_{i=1}^M \mathbf{I}[c_i = k] x_i}{\sum_{i=1}^M \mathbf{I}[c_i = k]}, \quad (8)$$

where  $\mathbf{I}[\cdot]$  is the indicator function and  $\tilde{z}_k$  denotes the iteratively updated cluster center.

After iterative refinement, we perform *cluster reselection* by selecting representative tokens as  $x_k^* = x_{i^*}$ ,  $i^* = \arg \max_{i:c_i=k} \text{sim}_{ik}$ , to obtain the final compact token set  $X_{\text{out}} = \{x_k^*\}_{k=1}^K$ . By applying text-aware token cluster selection only when significant distribution deviation occurs, TATCS maintains feature distribution consistency while improving the semantic representativeness of retained tokens under ultra-low token budget.

## 4 Experiments

### 4.1 Experiment Settings

**Models.** We evaluate the effectiveness of our proposed token pruning strategy under ultra-low token budget on a set of representative vision-language models, including LLaVA-1.5 (Liu et al., 2024a), LLaVA-NeXT (Liu et al., 2024b), Video-LLaVA (Lin et al., 2024), and Qwen2-VL (Wang et al., 2024b), covering both image and video understanding tasks. Specifically, image understanding is evaluated on five widely used benchmarks: GQA (Hudson and Manning, 2019), MME (Fu et al., 2023), POPE (Li et al., 2023b), SQA (Lu et al., 2022), and TextVQA (Singh et al., 2019), while video understanding is evaluated on TGIF (Jang et al., 2017), MSVD (Chen and Dolan, 2011), and MSRVT (Xu et al., 2016). We compare against a set of recent competitive methods, including VisionZip (Yang et al., 2025a), HoloV (Zou et al., 2025), FlowCut (Tong et al., 2025), PRUNESID (Fang et al., 2026), and SCOPE (Deng et al., 2025).

**Implementation Details.** Our method is entirely training-free and operates exclusively at inference time. For ACGR, pruning is applied every two Transformer layers in the vision encoder, progressively and uniformly reducing the token budget from the initial visual token number  $N$  to the target budget  $K$ , while using  $k_n = 5$ , a spatial decay factor  $\tau = 10$ , and a fusion coefficient  $\alpha = 0.1$  across all experiments. In TATCS, which is only potentially activated at the final pruning layer, reselection is triggered when the threshold  $\delta = 0.1$  is exceeded. Meanwhile, text features are extracted either from the text encoder aligned with the visual

embedding space, when available (Radford et al., 2021), or otherwise from the aligned LLM text representations. All methods are evaluated under identical backbone and inference settings to ensure a fair comparison.

### 4.2 Main Results

**Results on LLaVA 1.5.** Table 1 reports the performance of different methods on LLaVA-1.5-7B under varying token budgets. As the token budget decreases, the performance advantage of our method becomes progressively more pronounced. Specifically, our method achieves 96.3% accuracy at 64 tokens, surpassing the strongest method by 0.5%. The gain further increases to 0.7% at 32 tokens and reaches 2.7% at 16 tokens. These results highlight the effectiveness and robustness of our method, particularly in ultra-low token budget.

Moreover, existing methods degrade more rapidly as the token budget becomes more restrictive, whereas our method remains more stable. When the token budget is reduced from 64 to 16, the accuracy of SCOPE declines from 95.8% to 89.4%, while our method only drops from 96.3% to 92.1%. Even more pronounced degradation is observed in FlowCut, whose accuracies decrease from 94.4% to 82.3%. These results suggest that our method is more robust under ultra-low token pruning and better preserves representation quality.

Furthermore, under the ultra-low token budget of 16 tokens, our method achieves the best performance across all evaluated benchmarks. In particular, it reaches 81.5% on POPE, outperforming SCOPE by 4.6%, and achieves 55.1% on GQA, which is also higher than SCOPE at 53.4%. These results show that our method exhibits slower performance degradation as the token budget becomes more aggressive. Overall, the results demonstrate that our method consistently maintains stronger performance than existing approaches under ultra-low token budget.

**Results on LLaVA-NeXT.** We further evaluate our method on LLaVA-NeXT-7B, which contains up to 2880 visual tokens, posing a higher risk of feature distribution inconsistency under ultra-low token pruning.

As shown in Table 2, our method also achieves strong performance on LLaVA-NeXT-7B, which contains substantially more visual tokens. Under moderate pruning with 160 retained tokens, different methods achieve relatively similar performance,

Table 1: Performance comparison under different visual token settings on LLaVA-1.5-7B. The vanilla number of visual tokens is 576, and the last column reports the average accuracy proportion w.r.t. the vanilla. The entries marked with † are reported from the corresponding original papers.

Method	GQA	MME	POPE	SQA	TextVQA	Avg.
<i>Upper Bound, 576 Tokens (100.0%)</i>						
Vanilla	61.9	1862	85.9	69.5	58.2	100.0%
<i>Retain 64 Tokens (↓ 88.9%)</i>						
VisionZip	55.1 <sup>†</sup>	1690 <sup>†</sup>	80.9 <sup>†</sup>	69.0 <sup>†</sup>	55.5 <sup>†</sup>	93.7%
HoloV	55.3 <sup>†</sup>	1715 <sup>†</sup>	80.3 <sup>†</sup>	<b>69.5<sup>†</sup></b>	55.4 <sup>†</sup>	94.0%
FlowCut	55.6 <sup>†</sup>	<b>1744<sup>†</sup></b>	80.4 <sup>†</sup>	69.1 <sup>†</sup>	55.6 <sup>†</sup>	94.4%
PRUNESID	57.1 <sup>†</sup>	1733 <sup>†</sup>	83.8 <sup>†</sup>	67.8 <sup>†</sup>	54.2 <sup>†</sup>	94.7%
SCOPE	58.3 <sup>†</sup>	1698 <sup>†</sup>	83.9 <sup>†</sup>	<b>68.6<sup>†</sup></b>	<b>56.6<sup>†</sup></b>	95.8%
Ours	<b>58.5</b>	1719	<b>86.5</b>	68.3	55.7	<b>96.3%</b>
<i>Retain 32 Tokens (↓ 94.4%)</i>						
VisionZip	51.9	1581	74.7	68.8	53.1	89.2%
HoloV	52.8	1598	76.1	<b>68.8</b>	53.7	90.2%
FlowCut	51.9	1558	75.5	68.3	52.6	88.8%
PRUNESID	54.8	1592	82.1	67.8	52.5	91.5%
SCOPE	56.4	<b>1655</b>	82.4	68.4	<b>54.8</b>	93.7%
Ours	<b>57.0</b>	1654	<b>85.0</b>	68.6	54.3	<b>94.4%</b>
<i>Retain 16 Tokens (↓ 97.2%)</i>						
VisionZip	47.0	1350	66.6	67.8	49.8	81.8%
HoloV	48.9	1444	70.6	68.1	50.7	84.8%
FlowCut	48.2	1357	71.1	67.2	47.4	82.3%
PRUNESID	50.3	1436	74.5	67.3	49.5	85.4%
SCOPE	53.4	1562	76.9	68.2	52.0	89.4%
Ours	<b>55.1</b>	<b>1624</b>	<b>81.5</b>	<b>69.3</b>	<b>52.1</b>	<b>92.1%</b>

while our method still slightly outperforms SCOPE in average accuracy, demonstrating that our method remains effective even when the original model contains substantially more visual tokens.

The advantage of our method becomes increasingly pronounced as the token budget decreases. At 80 and 40 retained tokens, our method surpasses SCOPE by 1.2% and 3.0% in average accuracy, respectively. Under the most aggressive setting with only 20 retained tokens, our method still preserves 80.7% of the upper-bound performance and exceeds all baselines by at least 4.7%, while competing methods are at or below 76.0%.

The gains are particularly evident on GQA, MME, and POPE. Under the 20 token setting, our method outperforms SCOPE by 4.1% on GQA and 8.2% on POPE. These results show that our method maintains stronger performance under extreme compression.

**Results on Video-LLaVA.** We further evaluate our method on Video-LLaVA under aggressive visual token pruning. Because video understanding requires capturing both spatial and temporal dependencies, it is more sensitive to token reduction.

As shown in Table 3, our method achieves the best average performance under both token budgets, retaining 79.52% and 69.89% of the vanilla

Table 2: Performance comparison under different visual token settings on LLaVA-NeXT-7B. The vanilla number of visual tokens is 2880, and the last column reports the average accuracy proportion w.r.t. the vanilla.

Method	GQA	MME	POPE	SQA	TextVQA	Avg.
<i>Upper Bound, 2880 Tokens (100.0%)</i>						
Vanilla	64.2	1842	86.4	70.2	61.3	100.0%
<i>Retain 160 Tokens (↓ 94.4%)</i>						
VisionZip	55.5 <sup>†</sup>	1630 <sup>†</sup>	84.2	<b>68.3<sup>†</sup></b>	56.2 <sup>†</sup>	92.3%
HoloV	57.2	1675	81.4	67.1	52.3	91.0%
FlowCut	57.6 <sup>†</sup>	1746 <sup>†</sup>	79.9 <sup>†</sup>	66.5	57.6 <sup>†</sup>	93.1%
PRUNESID	58.9 <sup>†</sup>	1704 <sup>†</sup>	76.9 <sup>†</sup>	67.1 <sup>†</sup>	<b>59.1</b>	93.1%
SCOPE	<b>60.0</b>	1700 <sup>†</sup>	83.5	67.4 <sup>†</sup>	56.8 <sup>†</sup>	94.2%
Ours	59.7	<b>1764</b>	<b>84.6</b>	67.5	55.3	<b>94.6%</b>
<i>Retain 80 Tokens (↓ 97.2%)</i>						
VisionZip	52.3	1534	75.2	<b>68.3</b>	53.4	87.2%
HoloV	48.7	1432	69.1	67.7	46.9	81.3%
FlowCut	54.9	1550	78.5	<b>68.3</b>	<b>55.2</b>	89.6%
PRUNESID	56.3	1642	78.9	66.8	49.9	88.9%
SCOPE	57.6	1636	79.1	68.2	53.0	90.7%
Ours	<b>58.7</b>	<b>1692</b>	<b>80.8</b>	67.1	53.3	<b>91.9%</b>
<i>Retain 40 Tokens (↓ 98.6%)</i>						
VisionZip	44.1	1150	62.4	65.5	47.0	74.7%
HoloV	44.3	1229	62.2	66.5	43.4	74.6%
FlowCut	50.7	1401	72.6	<b>68.7</b>	<b>50.3</b>	83.8%
PRUNESID	49.4	1261	66.1	67.5	45.6	78.5%
SCOPE	54.3	1515	73.0	68.4	48.4	85.5%
Ours	56.1	<b>1655</b>	<b>76.5</b>	66.7	50.0	<b>88.5%</b>
<i>Retain 20 Tokens (↓ 99.3%)</i>						
VisionZip	42.3	1134	65.2	67.3	43.4	73.9%
HoloV	41.2	1051	56.2	64.5	41.1	69.0%
FlowCut	40.6	1012	53.6	65.2	41.0	68.0%
PRUNESID	44.8	1002	54.3	67.0	39.0	69.2%
SCOPE	47.8	1298	60.4	67.3	42.4	76.0%
Ours	<b>51.9</b>	<b>1379</b>	<b>68.6</b>	<b>68.0</b>	<b>43.9</b>	<b>80.7%</b>

accuracy with only 128 and 64 visual tokens, respectively. In particular, our method shows clear advantages on TGIF, reaching 33.60% at 128 tokens and 30.57% at 64 tokens, outperforming SCOPE by 7.85% and 10.10%, respectively. It also consistently surpasses FlowCut across all datasets and token budgets. This suggests that even under aggressive pruning, our method preserves most of the original performance. This demonstrates the effectiveness of our framework on video language tasks. These findings indicate that substantial redundancy exists in video inputs, suggesting that aggressive token pruning can significantly improve the efficiency of video LLMs without causing severe performance degradation.

**Results on Qwen2-VL.** Table 4 presents the performance comparison on Qwen2-VL-7B under a 95% token reduction ratio. Our method achieves the best average performance of 89.3%, outperforming SCOPE and FlowCut by 1.5% and 3.5%, respectively, further demonstrating its effectiveness under ultra-low token budget. Moreover, our method achieves the best performance on GQA, MME, POPE, and SQA under ultra-low token bud-

Table 3: Performance comparison on Video-LLaVA under different visual token settings. The vanilla number of visual tokens is 2048, and the last column reports the average accuracy proportion w.r.t. the vanilla.

Method	TGIF	MSVD	MSRVTT	Avg.
<i>Upper Bound, 2048 Tokens (100.0%)</i>				
Vanilla	45.70	68.09	54.49	100.0%
<i>Retain 128 Tokens (↓ 93.8%)</i>				
FlowCut	29.39	46.16	37.45	66.95%
SCOPE	25.75	<b>60.06</b>	44.81	75.59%
Ours	<b>33.60</b>	52.76	<b>47.70</b>	<b>79.52%</b>
<i>Retain 64 Tokens (↓ 96.9%)</i>				
FlowCut	25.80	38.38	31.39	56.82%
SCOPE	20.47	<b>55.55</b>	<b>40.81</b>	67.09%
Ours	<b>30.57</b>	50.24	37.59	<b>69.89%</b>

Table 4: Performance comparison on Qwen2-VL-7B under 95% token reduction ratio. The last column reports the average accuracy proportion w.r.t. the vanilla.

Method	GQA	MME	POPE	SQA	TextVQA	Avg.
<i>Upper Bound (100.0%)</i>						
Vanilla	61.9	2302	88.8	84.6	81.3	100.0%
<i>Retain 5% Tokens (↓ 95.0%)</i>						
FlowCut	50.7	2036	79.3	78.2	62.4	85.8%
SCOPE	52.1	2085	81.2	78.3	<b>65.2</b>	87.8%
Ours	<b>54.3</b>	<b>2134</b>	<b>82.7</b>	<b>79.1</b>	64.6	<b>89.3%</b>

get, with particularly significant gains on GQA and MME, where it surpasses SCOPE by 2.2% and 49 points, respectively. These results demonstrate the consistent advantages of our approach across diverse multimodal understanding benchmarks.

### 4.3 Distribution Consistency and Ablation Analysis

**Distribution Consistency and Performance Correlation.** As illustrated in Fig. 1(a), reducing the token budget progressively increases the distribution deviation  $\kappa$ , while the downstream accuracy consistently decreases. Under moderate token budgets, both  $\kappa$  and accuracy change relatively smoothly. However, under ultra-low token budget,  $\kappa$  increases more rapidly and is accompanied by substantially larger performance degradation as the pruning budget is further reduced. This consistent trend indicates that larger distribution deviation is generally associated with lower accuracy under ultra-low token budget.

To further examine this relationship, Table 5 reports the absolute Pearson correlation coefficient between  $\kappa$  and downstream accuracy across token budgets ranging from 10 to 100. Strong corre-

Table 5: *Absolute* Pearson correlations between  $\kappa$  and accuracy across token budgets from 10 to 100.

Method	GQA	POPE	TextVQA
VisionZip	0.95	0.90	0.94
HoloV	0.86	0.95	0.82
FlowCut	0.96	0.99	0.96
PRUNESID	0.98	0.98	0.83
SCOPE	0.98	0.93	0.82
Ours	0.97	0.94	0.87

Table 6: Effect of ACGR and TATCS on performance and feature distribution consistency under ultra-low token pruning on LLaVA-1.5-7B. Each entry reports the *accuracy* /  $\kappa$ , where smaller  $\kappa$  (Eq. 1) indicates better feature distribution consistency.

Dataset	Tokens	w/o TATCS	w/o ACGR	ACGR+TATCS
GQA	16	37.8 / 1.06	50.5 / 0.78	<b>55.1 / 0.66</b>
	32	37.5 / 0.42	54.1 / 0.34	<b>57.0 / 0.21</b>
	64	37.7 / 0.43	56.7 / 0.15	<b>58.5 / 0.07</b>
POPE	16	50.2 / 1.07	72.9 / 0.85	<b>81.5 / 0.71</b>
	32	49.5 / 0.56	79.1 / 0.49	<b>85.0 / 0.23</b>
	64	50.2 / 0.46	82.6 / 0.10	<b>86.5 / 0.07</b>

lations are consistently observed across different benchmarks and pruning methods. In particular, the correlations on GQA remain above 0.86 for all methods, while POPE consistently achieves values at or above 0.90. TextVQA also exhibits high correlations ranging from 0.82 to 0.96. These results show that, under ultra-low token budget, the strong correlation between distribution deviation and accuracy exists across different pruning strategies and benchmarks. Therefore,  $\kappa$  can serve as an effective lightweight indicator for analyzing the behavior of aggressive compression.

**Ablation Analysis on ACGR and TATCS.** Removing ACGR consistently degrades performance, with the degradation becoming more severe as the token budget decreases, demonstrating the importance of ACGR during progressive pruning. As shown in Table 6, removing ACGR on POPE leads to accuracy drops of 3.9%, 5.9%, and 8.6% at token budgets of 64, 32, and 16, respectively. The progressively larger performance gap suggests that ACGR provides greater benefits under more aggressive pruning settings. These results indicate that enriching retained tokens with contextual information before token removal helps alleviate performance degradation under ultra-low token budget.

Removing TATCS causes substantial performance degradation across both datasets, highlighting its importance under ultra-low token pruning.

Table 7: Efficiency comparison on POPE under the 32 tokens setting.  $\Delta$  is the speed-up computed w.r.t. the vanilla. Our method clearly outperforms existing methods while maintaining comparable efficiency.

Method	Tokens	Accuracy	Time (s)	$\Delta$
Vanilla	576	85.9	2147	1.0 $\times$
VisionZip	32	74.7	901	2.4 $\times$
HoloV	32	76.1	876	<b>2.5</b> $\times$
FlowCut	32	75.5	<b>856</b>	<b>2.5</b> $\times$
PRUNESID	32	82.1	930	2.3 $\times$
SCOPE	32	82.4	884	2.4 $\times$
Ours	32	<b>85.0</b>	895	2.4 $\times$

Table 8: Performance drop after removing each component under ultra-low token pruning on LLaVA-1.5-7B. Rows "w/o  $s_i^{\text{cos}}$ ", "w/o  $s_i^{\text{var}}$ ", and "w/o  $s_i^{\text{abl}}$ " remove the corresponding ACGR score terms in Eq. 2; "w/o Text" removes the text-aware term of TATCS in Eq. 6.

Component	GQA			POPE		
	64	32	16	64	32	16
w/o $s_i^{\text{cos}}$	-0.2	-0.6	-0.3	-0.7	-1.1	-0.4
w/o $s_i^{\text{var}}$	-0.4	-0.3	-0.5	-0.4	-0.2	-0.1
w/o $s_i^{\text{abl}}$	-0.3	-0.1	-0.8	-0.7	-0.9	-0.5
w/o Text	-0.2	-0.2	-0.3	-0.5	-0.7	-0.5

As shown in Table 6, without TATCS, the accuracy on GQA remains around 37.5%-37.8% even as the token budget increases from 16 to 64, while a similar trend is observed on POPE, where the accuracy stays around 50% across different token budgets. Meanwhile,  $\kappa$  remains consistently high without TATCS. These results suggest that simply increasing the number of retained tokens does not necessarily improve performance under ultra-low token pruning. In contrast, TATCS substantially reduces  $\kappa$  and consistently improves accuracy across different token budgets, indicating its effectiveness under ultra-low token budget.

#### 4.4 Component and Efficiency Analysis

Table 7 compares our method with existing pruning approaches under the same 32 token budget. All pruning methods achieve about 2.3 $\times$  to 2.5 $\times$  acceleration over the Vanilla model, demonstrating the efficiency benefits of aggressive token reduction. Among them, our method achieves the highest accuracy of 85.0%, outperforming the strongest baseline SCOPE by 2.6% while maintaining a comparable inference time of 895s versus 884s. Although FlowCut is slightly faster, it suffers from noticeable accuracy degradation under the same ultra-low token budget. These results show that

our method achieves a better balance between accuracy and efficiency while maintaining comparable acceleration.

**Effect of Individual Components.** Table 8 shows that different ACGR score terms play complementary roles under ultra-low token pruning. Specifically,  $s_i^{\text{cos}}$  and  $s_i^{\text{var}}$  complement the  $s_i^{\text{cls}}$  score by modeling feature redundancy and transformation dynamics, respectively. In addition,  $s_i^{\text{abl}}$  further incorporates token influence through attention-ablation estimation, providing an additional importance signal beyond individual token saliency. This becomes increasingly beneficial under more aggressive pruning, where tokens with larger influence on other tokens may not always be assigned high importance by standard saliency-based estimation.

Removing the text-aware term in TATCS consistently degrades performance across various token budgets and benchmarks. As shown in Table 8, its removal causes performance drops on both GQA and POPE, with a more noticeable 0.7% decline on POPE at 32 tokens. This suggests that text-aware guidance becomes particularly important for hallucination-sensitive benchmarks such as POPE, where preserving text-relevant visual evidence is more critical for accurate prediction. Without text-aware guidance, visually salient but text-irrelevant tokens may dominate the clustering process, losing important visual information and thereby degrading accuracy under ultra-low token budget.

## 5 Conclusion

In this paper, we investigate ultra-low visual token pruning from the perspective of feature distribution consistency and show that aggressively reducing the token budget induces significant distribution shift in kept token representations, accompanied by performance degradation. To address this issue, we propose ACGR to transfer complementary contextual information from pruned tokens to retained anchor tokens before removal, and TATCS to mitigate distribution shift through text-aware representative token reselection. Extensive experiments on multiple vision-language models demonstrate that our method consistently achieves superior performance under ultra-low token budget, retaining 92.1% of the upper-bound performance on LLaVA-1.5-7B using only 16 visual tokens. Overall, our findings highlight the importance of preserving feature distribution consistency for ultra-low visual token pruning.

## Limitations

Although the proposed framework achieves strong performance under ultra-low token pruning, a noticeable gap still exists compared with using full visual tokens. Similar to existing pruning strategies, aggressive token compression inevitably causes partial information loss, making it difficult to fully preserve visual semantics under ultra-low token budget. We will explore more effective semantic preservation and adaptive token allocation strategies to further improve the balance between efficiency and performance.

## References

- Kazuki Adachi, Shin'Ya Yamaguchi, and Atsutoshi Kumagai. 2023. Covariance-aware feature alignment with pre-computed source statistics for test-time adaptation to multiple image corruptions. In *IEEE International Conference on Image Processing*, pages 800–804.
- Jean-Baptiste Alayrac, Jeff Donahue, Pauline Luc, Antoine Miech, Iain Barr, Yana Hasson, Karel Lenc, Arthur Mensch, Katherine Millican, Malcolm Reynolds, and 1 others. 2022. Flamingo: a visual language model for few-shot learning. In *Advances in Neural Information Processing Systems*, pages 23716–23736.
- Anurag Arnab, Mostafa Dehghani, Georg Heigold, Chen Sun, Mario Lučić, and Cordelia Schmid. 2021. Vivit: A video vision transformer. In *IEEE/CVF International Conference on Computer Vision*, pages 6836–6846.
- Vincent Arsigny, Pierre Fillard, Xavier Pennec, and Nicholas Ayache. 2006. Log-euclidean metrics for fast and simple calculus on diffusion tensors. *Magnetic Resonance in Medicine: An Official Journal of the International Society for Magnetic Resonance in Medicine*, 56(2):411–421.
- Max Bain, Arsha Nagrani, Gül Varol, and Andrew Zisserman. 2021. Frozen in time: A joint video and image encoder for end-to-end retrieval. In *IEEE/CVF International Conference on Computer Vision*, pages 1728–1738.
- Daniel Bolya, Cheng-Yang Fu, Xiaoliang Dai, Peizhao Zhang, Christoph Feichtenhofer, and Judy Hoffman. 2022. Token merging: Your vit but faster. *arXiv preprint arXiv:2210.09461*.
- Hila Chefer, Shir Gur, and Lior Wolf. 2021. Transformer interpretability beyond attention visualization. In *IEEE/CVF Conference on Computer Vision and Pattern Recognition*, pages 782–791.
- David Chen and William B Dolan. 2011. Collecting highly parallel data for paraphrase evaluation. In *Annual Meeting of the Association for Computational Linguistics: Human Language Technologies*, pages 190–200.
- Keqin Chen, Zhao Zhang, Weili Zeng, Richong Zhang, Feng Zhu, and Rui Zhao. 2023. Shikra: Unleashing multimodal llm’s referential dialogue magic. *arXiv preprint arXiv:2306.15195*.
- Liang Chen, Haozhe Zhao, Tianyu Liu, Shuai Bai, Junyang Lin, Chang Zhou, and Baobao Chang. 2024a. An image is worth 1/2 tokens after layer 2: Plug-and-play inference acceleration for large vision-language models. In *European Conference on Computer Vision*, pages 19–35.
- Xi Chen, Xiao Wang, Soravit Changpinyo, Anthony J Piergiovanni, Piotr Padlewski, Daniel Salz, Sebastian Goodman, Adam Grycner, Basil Mustafa, Lucas Beyer, and 1 others. 2022. Pali: A jointly-scaled multilingual language-image model. *arXiv preprint arXiv:2209.06794*.
- Yuan Chen, Zichen Wen, Yuzhou Wu, Xuyang Liu, Shuang Chen, Junpeng Ma, Weijia Li, Conghui He, and Linfeng Zhang. 2025. Ipcv: Information-preserving compression for mllm visual encoders. *arXiv preprint arXiv:2512.18747*.
- Zhe Chen, Jiannan Wu, Wenhai Wang, Weijie Su, Guo Chen, Sen Xing, Muyan Zhong, Qinglong Zhang, Xizhou Zhu, Lewei Lu, and 1 others. 2024b. Internvl: Scaling up vision foundation models and aligning for generic visual-linguistic tasks. In *IEEE/CVF Conference on Computer Vision and Pattern Recognition*, pages 24185–24198.
- Wenliang Dai, Junnan Li, Dongxu Li, Anthony Tiong, Junqi Zhao, Weisheng Wang, Boyang Li, Pascale N Fung, and Steven Hoi. 2023. Instructblip: Towards general-purpose vision-language models with instruction tuning. In *Advances in Neural Information Processing Systems*, pages 49250–49267.
- Mostafa Dehghani, Basil Mustafa, Josip Djolonga, Jonathan Heek, Matthias Minderer, Mathilde Caron, Andreas Steiner, Joan Puigcerver, Robert Geirhos, Ibrahim M Alabdulmohsin, and 1 others. 2023. Patch n’ pack: Navit, a vision transformer for any aspect ratio and resolution. In *Advances in Neural Information Processing Systems*, pages 2252–2274.
- Jinhong Deng, Wen Li, Joey Tianyi Zhou, and Yang He. 2025. Scope: Saliency-coverage oriented token pruning for efficient multimodal llms. *arXiv preprint arXiv:2510.24214*.
- Xiaoyi Dong, Pan Zhang, Yuhang Zang, Yuhang Cao, Bin Wang, Linke Ouyang, Songyang Zhang, Haodong Duan, Wenwei Zhang, Yining Li, and 1 others. 2024. Internlm-xcomposer2-4khd: A pioneering large vision-language model handling resolutions from 336 pixels to 4k hd. In *Advances in Neural Information Processing Systems*, pages 42566–42592.

- David C Dowson and B.V Landau. 1982. The fréchet distance between multivariate normal distributions. *Journal of multivariate analysis*, 12(3):450–455.
- Yuanzhi Duan, Yue Zhou, Peng He, Qiang Liu, Shukai Duan, and Xiaofang Hu. 2022. Network pruning via feature shift minimization. In *Asian Conference on Computer Vision*, pages 4044–4060.
- Mark Endo, Xiaohan Wang, and Serena Yeung-Levy. 2025. Feather the throttle: Revisiting visual token pruning for vision-language model acceleration. In *IEEE/CVF International Conference on Computer Vision*, pages 22826–22835.
- Zhengyao Fang, Pengyuan Lyu, Chengquan Zhang, Guangming Lu, Jun Yu, and Wenjie Pei. 2026. Prune redundancy, preserve essence: Vision token compression in vlms via synergistic importance-diversity. *arXiv preprint arXiv:2603.09480*.
- Mohsen Fayyaz, Soroush Abbasi Koohpayegani, Farnoush Rezaei Jafari, Sunando Sengupta, Hamid Reza Vaezi Joze, Eric Sommerlade, Hamed Pirsiavash, and Jürgen Gall. 2022. Adaptive token sampling for efficient vision transformers. In *European Conference on Computer Vision*, pages 396–414.
- Chaoyou Fu, Peixian Chen, Yunhang Shen, Yulei Qin, Mengdan Zhang, Xu Lin, Jinrui Yang, Xiawu Zheng, Ke Li, Xing Sun, Yunsheng Wu, Rongrong Ji, Caifeng Shan, and Ran He. 2023. Mme: A comprehensive evaluation benchmark for multimodal large language models. *arXiv preprint arXiv:2306.13394*.
- Zonghao Guo, Ruyi Xu, Yuan Yao, Junbo Cui, Zanlin Ni, Chunjiang Ge, Tat-Seng Chua, Zhiyuan Liu, and Gao Huang. 2024. Llava-uhd: an lmm perceiving any aspect ratio and high-resolution images. In *European Conference on Computer Vision*, pages 390–406.
- Shaohan Huang, Li Dong, Wenhui Wang, Yaru Hao, Saksham Singhal, Shuming Ma, Tengchao Lv, Lei Cui, Owais Khan Mohammed, Barun Patra, and 1 others. 2023. Language is not all you need: Aligning perception with language models. In *Advances in Neural Information Processing Systems*, pages 72096–72109.
- Xun Huang and Serge Belongie. 2017. Arbitrary style transfer in real-time with adaptive instance normalization. In *IEEE/CVF International Conference on Computer Vision*, pages 1501–1510.
- Drew A Hudson and Christopher D Manning. 2019. Gqa: A new dataset for real-world visual reasoning and compositional question answering. In *IEEE/CVF Conference on Computer Vision and Pattern Recognition*, pages 6700–6709.
- Sergey Ioffe and Christian Szegedy. 2015. Batch normalization: Accelerating deep network training by reducing internal covariate shift. In *International Conference on Machine Learning*, pages 448–456.
- Ryuto Ishibashi and Lin Meng. 2025. Automatic pruning rate adjustment for dynamic token reduction in vision transformer. *Applied Intelligence*, 55(5):342.
- Yunseok Jang, Yale Song, Youngjae Yu, Youngjin Kim, and Gunhee Kim. 2017. Tgif-qa: Toward spatio-temporal reasoning in visual question answering. In *IEEE/CVF Conference on Computer Vision and Pattern Recognition*, pages 2758–2766.
- Ahmadreza Jeddi, Negin Baghbanzadeh, Elham Dolatabadi, and Babak Taati. 2025. Similarity-aware token pruning: Your vlm but faster. *arXiv preprint arXiv:2503.11549*.
- Yutao Jiang, Qiong Wu, Wenhao Lin, Wei Yu, and Yiyi Zhou. 2025. What kind of visual tokens do we need? training-free visual token pruning for multi-modal large language models from the perspective of graph. In *AAAI Conference on Artificial Intelligence*, pages 4075–4083.
- Youngeun Kim, Youjia Zhang, Huiling Liu, Aecheon Jung, Sunwoo Lee, and Sungeun Hong. 2025. Zoo-prune: Training-free token pruning via zeroth-order gradient estimation in vision-language models. *arXiv preprint arXiv:2509.24837*.
- Ao Li, Yuxiang Duan, Jinghui Zhang, Congbo Ma, Yutong Xie, Gustavo Carneiro, Mohammad Yaqub, and Hu Wang. 2025a. Transprune: Token transition pruning for efficient large vision-language model. *arXiv preprint arXiv:2507.20630*.
- Bo Li, Yuanhan Zhang, Dong Guo, Renrui Zhang, Feng Li, Hao Zhang, Kaichen Zhang, Peiyuan Zhang, Yanwei Li, and Ziwei Liu. 2024a. Llava-onevision: Easy visual task transfer. *arXiv preprint arXiv:2408.03326*.
- Feng Li, Renrui Zhang, Hao Zhang, Yuanhan Zhang, Bo Li, Wei Li, Zejun Ma, and Chunyuan Li. 2024b. Llava-next-interleave: Tackling multi-image, video, and 3d in large multimodal models. *arXiv preprint arXiv:2407.07895*.
- Junnan Li, Dongxu Li, Silvio Savarese, and Steven Hoi. 2023a. Blip-2: Bootstrapping language-image pre-training with frozen image encoders and large language models. In *International Conference on Machine Learning*, pages 19730–19742.
- Kaiyuan Li, Xiaoyue Chen, Chen Gao, Yong Li, and Xinlei Chen. 2025b. Balanced token pruning: Accelerating vision language models beyond local optimization. *arXiv preprint arXiv:2505.22038*.
- Peihua Li, Jiangtao Xie, Qilong Wang, and Zilin Gao. 2018. Towards faster training of global covariance pooling networks by iterative matrix square root normalization. In *IEEE/CVF Conference on Computer Vision and Pattern Recognition*, pages 947–955.
- Yanwei Li, Chengyao Wang, and Jiaya Jia. 2024c. Llama-vid: An image is worth 2 tokens in large language models. In *European Conference on Computer Vision*, pages 323–340.

- Yifan Li, Yifan Du, Kun Zhou, Jinpeng Wang, Xin Zhao, and Ji-Rong Wen. 2023b. Evaluating object hallucination in large vision-language models. In *Conference on Empirical Methods in Natural Language Processing*, pages 292–305.
- Chen Liang, Weihua Chen, Xin Zhao, Junyan Wang, Lijun Cao, and Junge Zhang. 2025. Distribution optimization under gaussian hypothesis for domain adaptive semantic segmentation. In *IEEE/CVF Winter Conference on Applications of Computer Vision*, pages 9280–9290.
- Youwei Liang, Chongjian Ge, Zhan Tong, Yibing Song, Jue Wang, and Pengtao Xie. 2022. Not all patches are what you need: Expediting vision transformers via token reorganizations. *arXiv preprint arXiv:2202.07800*.
- Bin Lin, Yang Ye, Bin Zhu, Jiayi Cui, Munan Ning, Peng Jin, and Li Yuan. 2024. Video-llava: Learning united visual representation by alignment before projection. In *Conference on Empirical Methods in Natural Language Processing*, pages 5971–5984.
- Haotian Liu, Chunyuan Li, Yuheng Li, and Yong Jae Lee. 2024a. Improved baselines with visual instruction tuning. In *IEEE/CVF Conference on Computer Vision and Pattern Recognition*, pages 26296–26306.
- Haotian Liu, Chunyuan Li, Yuheng Li, Bo Li, Yuanhan Zhang, Sheng Shen, and Yong Jae Lee. 2024b. Llava-next: Improved reasoning, ocr, and world knowledge.
- Haotian Liu, Chunyuan Li, Qingyang Wu, and Yong Jae Lee. 2023. Visual instruction tuning. In *Advances in Neural Information Processing Systems*, pages 34892–34916.
- Sifan Long, Zhen Zhao, Jimin Pi, Shengsheng Wang, and Jingdong Wang. 2023. Beyond attentive tokens: Incorporating token importance and diversity for efficient vision transformers. In *IEEE/CVF Conference on Computer Vision and Pattern Recognition*, pages 10334–10343.
- Pan Lu, Swaroop Mishra, Tanglin Xia, Liang Qiu, Kai-Wei Chang, Song-Chun Zhu, Oyvind Tafjord, Peter Clark, and Ashwin Kalyan. 2022. Learn to explain: Multimodal reasoning via thought chains for science question answering. In *Advances in Neural Information Processing Systems*, pages 2507–2521.
- Seungwhan Moon, Andrea Madotto, Zhaojiang Lin, Tushar Nagarajan, Matt Smith, Shashank Jain, Chun-Fu Yeh, Prakash Murugesan, Peyman Heidari, Yue Liu, and 1 others. 2024. Anymal: An efficient and scalable any-modality augmented language model. In *Conference on Empirical Methods in Natural Language Processing*, pages 1314–1332.
- Alec Radford, Jong Wook Kim, Chris Hallacy, Aditya Ramesh, Gabriel Goh, Sandhini Agarwal, Girish Sastry, Amanda Askell, Pamela Mishkin, and Jack Clark. 2021. Learning transferable visual models from natural language supervision. In *International Conference on Machine Learning*, pages 8748–8763.
- Yongming Rao, Wenliang Zhao, Benlin Liu, Jiwen Lu, Jie Zhou, and Cho-Jui Hsieh. 2021. Dynamicvit: Efficient vision transformers with dynamic token sparsification. In *Advances in Neural Information Processing Systems*, pages 13937–13949.
- Yuzhang Shang, Mu Cai, Bingxin Xu, Yong Jae Lee, and Yan Yan. 2025. Llava-prumerge: Adaptive token reduction for efficient large multimodal models. In *IEEE/CVF International Conference on Computer Vision*, pages 22857–22867.
- Amanpreet Singh, Vivek Natarajan, Meet Shah, Yu Jiang, Xinlei Chen, Dhruv Batra, Devi Parikh, and Marcus Rohrbach. 2019. Towards vqa models that can read. In *IEEE/CVF Conference on Computer Vision and Pattern Recognition*, pages 8317–8326.
- Baochen Sun, Jiashi Feng, and Kate Saenko. 2017. Correlation alignment for unsupervised domain adaptation. In *Domain Adaptation in Computer Vision Applications*, pages 153–171. Springer.
- Baochen Sun and Kate Saenko. 2016. Deep coral: Correlation alignment for deep domain adaptation. In *European Conference on Computer Vision*, pages 443–450.
- Chen Sun, Austin Myers, Carl Vondrick, Kevin Murphy, and Cordelia Schmid. 2019. Videobert: A joint model for video and language representation learning. In *IEEE/CVF International Conference on Computer Vision*, pages 7464–7473.
- Yizheng Sun, Yanze Xin, Hao Li, Jingyuan Sun, Chenghua Lin, and Riza Theresa Batista-Navarro. 2025. Lvpruning: An effective yet simple language-guided vision token pruning approach for multimodal large language models. In *Findings of the Association for Computational Linguistics*, pages 4299–4308.
- Mukund Sundararajan, Ankur Taly, and Qiqi Yan. 2017. Axiomatic attribution for deep networks. In *International Conference on Machine Learning*, pages 3319–3328.
- Xudong Tan, Peng Ye, Chongjun Tu, Jianjian Cao, Yaolin Yang, Lin Zhang, Dongzhan Zhou, and Tao Chen. 2025. Tokencarve: Information-preserving visual token compression in multimodal large language models. *arXiv preprint arXiv:2503.10501*.
- Jintao Tong, Wenwei Jin, Pengda Qin, Anqi Li, Yixiong Zou, Yuhong Li, Yuhua Li, and Ruixuan Li. 2025. Flowcut: Rethinking redundancy via information flow for efficient vision-language models. *arXiv preprint arXiv:2505.19536*.
- Dmitry Ulyanov, Andrea Vedaldi, and Victor Lempitsky. 2016. Instance normalization: The missing ingredient for fast stylization. *arXiv preprint arXiv:1607.08022*.

- Hongjie Wang, Bhishma Dedhia, and Niraj K Jha. 2024a. Zero-tprune: Zero-shot token pruning through leveraging of the attention graph in pre-trained transformers. In *IEEE/CVF Conference on Computer Vision and Pattern Recognition*, pages 16070–16079.
- Peng Wang, Shuai Bai, Sinan Tan, Shijie Wang, Zhihao Fan, Jinze Bai, Keqin Chen, Xuejing Liu, Jialin Wang, and Wenbin Ge. 2024b. Qwen2-vl: Enhancing vision-language model’s perception of the world at any resolution. *arXiv preprint arXiv:2409.12191*.
- Weihan Wang, Qingsong Lv, Wenmeng Yu, Wenyi Hong, Ji Qi, Yan Wang, Junhui Ji, Zhuoyi Yang, Lei Zhao, Xixuan Song, and 1 others. 2024c. Cogvlm: Visual expert for pretrained language models. In *Advances in Neural Information Processing Systems*, pages 121475–121499.
- Wenhai Wang, Zhe Chen, Xiaokang Chen, Jiannan Wu, Xizhou Zhu, Gang Zeng, Ping Luo, Tong Lu, Jie Zhou, Yu Qiao, and 1 others. 2023. Visionllm: Large language model is also an open-ended decoder for vision-centric tasks. In *Advances in Neural Information Processing Systems*, pages 61501–61513.
- Junyi Wu, Bin Duan, Weitai Kang, Hao Tang, and Yan Yan. 2024. Token transformation matters: Towards faithful post-hoc explanation for vision transformer. In *IEEE/CVF Conference on Computer Vision and Pattern Recognition*, pages 10926–10935.
- Jun Xu, Tao Mei, Ting Yao, and Yong Rui. 2016. Msr-vtt: A large video description dataset for bridging video and language. In *IEEE/CVF Conference on Computer Vision and Pattern Recognition*, pages 5288–5296.
- Senqiao Yang, Yukang Chen, Zhuotao Tian, Chengyao Wang, Jingyao Li, Bei Yu, and Jiaya Jia. 2025a. Visionzip: Longer is better but not necessary in vision language models. In *IEEE/CVF Conference on Computer Vision and Pattern Recognition*, pages 19792–19802.
- Sihan Yang, Runsen Xu, Chenhang Cui, Tai Wang, Dahua Lin, and Jiangmiao Pang. 2025b. Vflowopt: A token pruning framework for llms with visual information flow-guided optimization. In *IEEE/CVF International Conference on Computer Vision*, pages 23924–23934.
- Qinghao Ye, Haiyang Xu, Guohai Xu, Jiabo Ye, Ming Yan, Yiyang Zhou, Junyang Wang, Anwen Hu, Pengcheng Shi, Yaya Shi, and 1 others. 2023. mplug-owl: Modularization empowers large language models with multimodality. *arXiv preprint arXiv:2304.14178*.
- Hanxun Yu, Wentong Li, Xuan Qu, Song Wang, Junbo Chen, and Jianke Zhu. 2026. Visiontrim: Unified vision token compression for training-free mllm acceleration. *arXiv preprint arXiv:2601.22674*.
- Ce Zhang, Kaixin Ma, Tianqing Fang, Wenhao Yu, Hongming Zhang, Zhisong Zhang, Yaqi Xie, Kattia Sycara, Haitao Mi, and Dong Yu. 2025a. Vs-can: Rethinking visual token reduction for efficient large vision-language models. *arXiv preprint arXiv:2505.22654*.
- Hao Zhang, Mengsi Lyu, Chenrui He, Yulong Ao, and Yonghua Lin. 2025b. Trimtokenator: Towards adaptive visual token pruning for large multimodal models. *arXiv preprint arXiv:2509.00320*.
- Jianwei Zhang, Chaoning Zhang, Sihan Cao, Wang Liu, Pengcheng Zheng, Jiabin Huang, Caiyan Qin, Yalan Ye, Wei Dong, and Yang Yang. 2026. Rcp: Representation consistency pruner for mitigating distribution shift in large vision-language models. *arXiv preprint arXiv:2604.04972*.
- Qizhe Zhang, Aosong Cheng, Ming Lu, Renrui Zhang, Zhiyong Zhuo, Jiajun Cao, Shaobo Guo, Qi She, and Shanghang Zhang. 2025c. Beyond text-visual attention: Exploiting visual cues for effective token pruning in vlms. In *IEEE/CVF International Conference on Computer Vision*, pages 20857–20867.
- Yufeng Zhang, Jialu Pan, Li Ken Li, Wanwei Liu, Zhenbang Chen, Xinwang Liu, and Ji Wang. 2023. On the properties of kullback-leibler divergence between multivariate gaussian distributions. In *Advances in Neural Information Processing Systems*, pages 58152–58165.
- Deyao Zhu, Xiaoqian Shen, Xiang Li, and Mohamed Elhoseiny. 2024. Minigt-4: Enhancing vision-language understanding with advanced large language models. In *International Conference on Learning Representations*, pages 18378–18394.
- Xin Zou, Di Lu, Yizhou Wang, Yibo Yan, Yuanhuiyi Lyu, Xu Zheng, Linfeng Zhang, and Xuming Hu. 2025. Don’t just chase “highlighted tokens” in mllms: Revisiting visual holistic context retention. *arXiv preprint arXiv:2510.02912*.

## A Detailed Definitions of Token Importance Scores

To better assess token importance under ultra-low token budget, we combine multiple complementary criteria from different perspectives, including semantic relevance, redundancy suppression, feature transformation dynamics, and attention interaction effects. Given the patch tokens in the current layer  $X = \{x_i\}_{i=1}^M$ , the overall importance score of token  $x_i$  is defined as

$$s_i = s_i^{\text{cls}} + s_i^{\text{cos}} + s_i^{\text{var}} + s_i^{\text{abl}}. \quad (9)$$

**CLS relevance score.** To estimate the semantic importance of visual tokens, we introduce a CLS-guided relevance score based on the attention from the CLS token to each image patch. Tokens receiving higher CLS attention are regarded as more semantically informative and are thus more likely to be preserved during pruning (Zhang et al., 2025c; Liang et al., 2022; Long et al., 2023). Let  $A_{0,i}^{(h)}$  denote the attention weight from the CLS token to patch  $i$  at head  $h$ , where  $H$  is the number of attention heads. We first average the attention weights across heads and then normalize them across all tokens:

$$\alpha_i^{\text{cls}} = \frac{1}{H} \sum_{h=1}^H A_{0,i}^{(h)}. \quad (10)$$

$$s_i^{\text{cls}} = \frac{\alpha_i^{\text{cls}}}{\sum_{j=1}^M \alpha_j^{\text{cls}} + \varepsilon}. \quad (11)$$

**Cosine non-redundancy score.** To suppress redundancy among visual tokens, we measure the average cosine similarity between each token and all remaining tokens. Tokens that are less similar to others are considered to contain more unique information and are therefore assigned higher non-redundancy scores (Bolya et al., 2022; Jeddi et al., 2025; Wang et al., 2024a). Specifically, we compute the average cosine similarity of each token to all other tokens and transform it into a non-redundancy score:

$$c_i = 1 - \frac{1}{M-1} \sum_{\substack{j=1 \\ j \neq i}}^M \cos(x_i, x_j). \quad (12)$$

$$s_i^{\text{cos}} = \frac{c_i}{\sum_{j=1}^M c_j + \varepsilon}. \quad (13)$$

**Transformation variation score.** Tokens exhibiting larger feature updates through the attention and FFN branches are considered to encode richer semantic information and are therefore assigned higher importance scores (Ishibashi and Meng, 2025; Wu et al., 2024). This component follows the transition-based perspective in TransPrune (Li et al., 2025a). Let  $x_i^{\text{in}}$ ,  $x_i^{\text{att}}$ , and  $x_i^{\text{ffn}}$  denote the patch feature at the layer input, after the attention branch, and after the FFN branch in the same layer, respectively. We first measure the transformation magnitude of token  $i$  in the attention and FFN branches by cosine distance:

$$d_i^{\text{att}} = 1 - \cos(x_i^{\text{in}}, x_i^{\text{att}}), \quad d_i^{\text{ffn}} = 1 - \cos(x_i^{\text{in}}, x_i^{\text{ffn}}). \quad (14)$$

The distances are then normalized across all patch tokens with a softmax operation:

$$p_i^{\text{att}} = \frac{\exp(d_i^{\text{att}})}{\sum_{j=1}^M \exp(d_j^{\text{att}})}, \quad p_i^{\text{ffn}} = \frac{\exp(d_i^{\text{ffn}})}{\sum_{j=1}^M \exp(d_j^{\text{ffn}})}. \quad (15)$$

To further account for the change in feature magnitude, we compute the norm ratios:

$$r_i^{\text{att}} = \frac{\|x_i^{\text{att}}\|_2}{\|x_i^{\text{in}}\|_2 + \varepsilon}, \quad r_i^{\text{ffn}} = \frac{\|x_i^{\text{ffn}}\|_2}{\|x_i^{\text{in}}\|_2 + \varepsilon}. \quad (16)$$

The final transformation variation score is computed by combining the normalized transformation weights and magnitude ratios:

$$s_i^{\text{var}} = p_i^{\text{att}} r_i^{\text{att}} + p_i^{\text{ffn}} r_i^{\text{ffn}}. \quad (17)$$

**Attention-ablation impact score.** Some tokens may appear locally unimportant while still exerting strong influence on other token representations through Transformer attention interactions (Chefer et al., 2021; Sundararajan et al., 2017). To capture this effect, we estimate token importance by measuring how much the representations of other tokens change after removing a target token from the attention process. Tokens inducing larger representation variations are considered more important for contextual information propagation.

For a fixed attention head, the attention output of token  $i$  is

$$a_i = \sum_{j=1}^M \alpha_{ij} v_j, \quad (18)$$

where  $M$  is the number of patch tokens,  $\alpha_{ij}$  is the attention weight from token  $i$  to token  $j$ , and  $v_j$  is the value vector of token  $j$ .

If token  $k$  is removed, the remaining attention weights are renormalized as

$$\tilde{a}_i^{(-k)} = \sum_{j \neq k} \frac{\alpha_{ij}}{1 - \alpha_{ik} + \varepsilon} v_j = \frac{a_i - \alpha_{ik} v_k}{1 - \alpha_{ik} + \varepsilon}, \quad (19)$$

where  $\varepsilon$  is a small constant for numerical stability. The resulting output change is approximated by

$$\Delta a_i^{(k)} = \tilde{a}_i^{(-k)} - a_i \approx \frac{\alpha_{ik}}{1 - \alpha_{ik} + \varepsilon} (a_i - v_k). \quad (20)$$

We estimate the influence of token  $k$  on token  $i$  as

$$\hat{I}_{k \rightarrow i} = \frac{\alpha_{ik}}{1 - \alpha_{ik} + \varepsilon} \|a_i - v_k\|_2. \quad (21)$$

To avoid re-running the Transformer for each removed token, we further use a one-pass proxy:

$$I_{k \rightarrow i} = \frac{\bar{\alpha}_{ik}}{1 - \bar{\alpha}_{ik} + \varepsilon} \cdot \|y_i\|_2 \cdot \|\bar{v}_k\|_2, \quad (22)$$

where  $H$  is the number of attention heads,  $\bar{\alpha}_{ik}$  is the head-averaged attention weight,  $\bar{v}_k = \frac{1}{H} \sum_{h=1}^H v_{h,k}$ , and  $y_i$  is the current-layer hidden feature of token  $i$  obtained from the same forward pass.

Finally, the attention-ablation importance score is computed as

$$s_k^{\text{abl}} = \frac{1}{M-1} \sum_{\substack{i=1 \\ i \neq k}}^M I_{k \rightarrow i}. \quad (23)$$

## B Distribution Consistency Metric

Existing pruning strategies are generally importance-oriented or coverage-oriented, yet both tend to become unstable under ultra-low token budget (Fayyaz et al., 2022). As the token budget decreases, retained tokens progressively deviate from the original feature distribution (Rao et al., 2021), leading to degraded multimodal reasoning (Ioffe and Szegedy, 2015). Motivated by this observation, we revisit ultra-low token pruning from the perspective of distribution consistency between retained and full token representations.

A common way to measure distribution discrepancy is through divergence metrics such as KL divergence or Wasserstein distance (Dowson and Landau, 1982; Sun and Saenko, 2016). However, these methods typically require covariance inversion, eigendecomposition, or determinant computation, leading to considerable computational overhead and numerical instability for runtime token

pruning (Arsigny et al., 2006). Instead of estimating exact probability divergence, we adopt a lightweight distribution consistency approximation based on first- and second-order feature statistics:

$$\mathcal{D}(X_k, X_f) = \frac{\text{Tr}(\Sigma_k) + d \text{Var}(\mu_k)}{\text{Tr}(\Sigma_f) + d \text{Var}(\mu_f)}, \quad (24)$$

$$\kappa = |\mathcal{D}(X_k, X_f) - 1|,$$

where  $X_f$  and  $X_k$  denote the full token and kept token representations, respectively.

Here,  $\text{Tr}(\Sigma)$  denotes the trace of the covariance matrix and serves as a lightweight approximation of second-order feature statistics, reflecting the overall feature dispersion (Sun et al., 2017; Li et al., 2018), while  $\text{Var}(\mu)$  measures the variance of channel-wise mean activations and reflects shifts in channel-wise feature responses (Huang and Belongie, 2017; Ulyanov et al., 2016; Adachi et al., 2023). Since  $\text{Tr}(\Sigma)$  accumulates variance across feature dimensions, multiplying  $\text{Var}(\mu)$  by  $d$  balances the scales of first- and second-order statistics.

The ratio formulation provides a scale-normalized comparison between kept and full token representations. When the kept tokens preserve distribution consistency with the original tokens representation,  $\mathcal{D}(X_k, X_f)$  approaches 1, yielding a smaller  $\kappa$ . Therefore,  $\kappa$  is not intended as a strict probability divergence metric, but rather as a lightweight proxy for distribution deviation under ultra-low token pruning.

Although  $\kappa$  does not explicitly characterize representation geometry or fine-grained semantic structure, it provides an efficient empirical indicator of whether aggressive pruning introduces substantial statistical distribution deviation during inference. As shown in Table 5, larger  $\kappa$  consistently correlates with more severe downstream accuracy degradation under ultra-low token budget. Motivated by this observation, we use  $\kappa$  as an adaptive trigger signal for TATCS, which is activated only when the estimated distribution deviation exceeds a predefined threshold, thereby dynamically mitigating distribution shift in the retained token features.

## C Visualization of Kept Tokens

Fig. 3 and Fig. 4 compare token selection under 64 token budget on LLaVA-1.5-7B. FlowCut focuses on salient local regions, while SCOPE favors spatial coverage. By maintaining feature distribution consistency, our method preserves both semantic and contextual information, resulting in a more representative token subset.

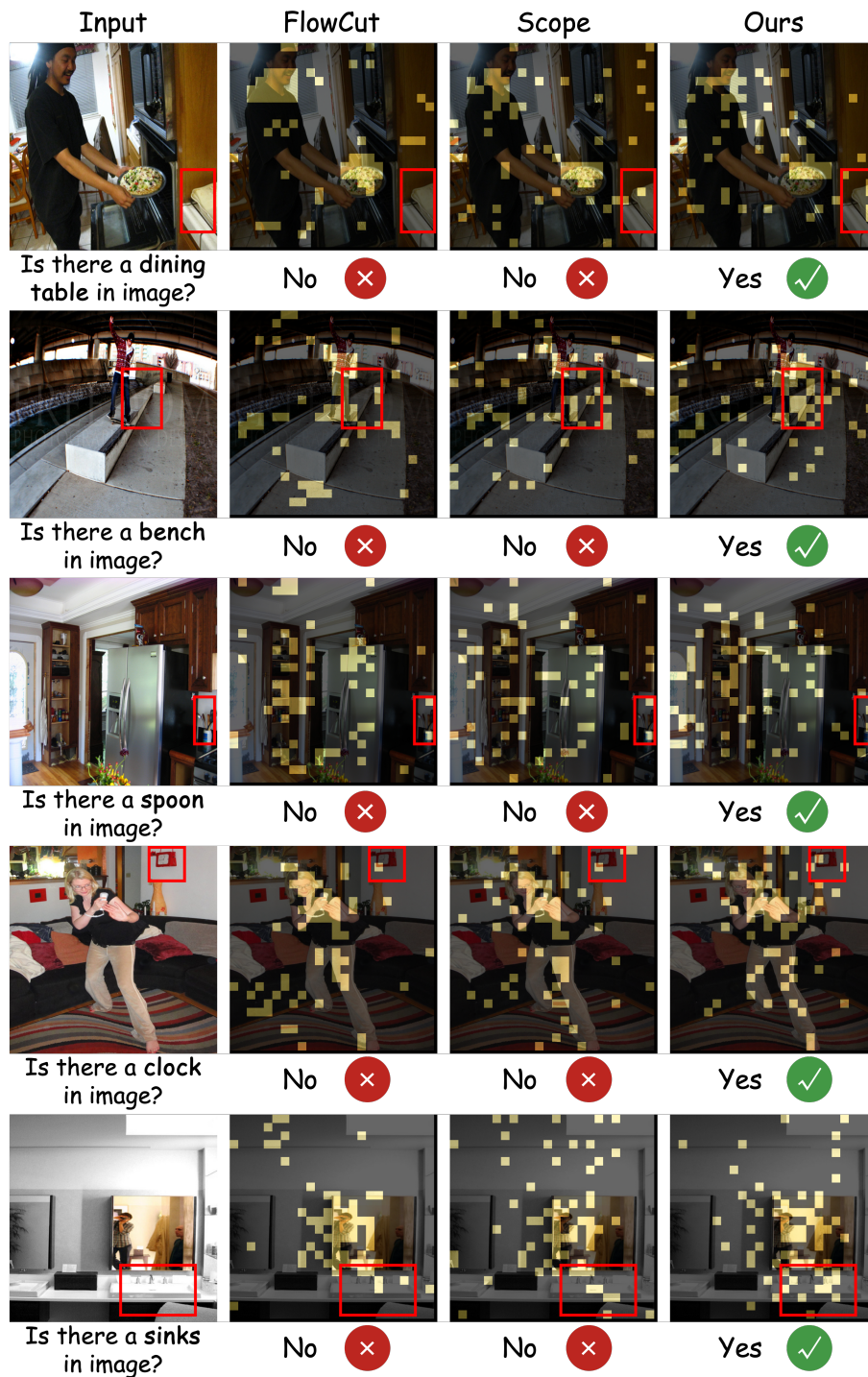


Figure 3: Qualitative visualization of selected visual tokens under a token budget of 64 on LLaVA-1.5-7B.

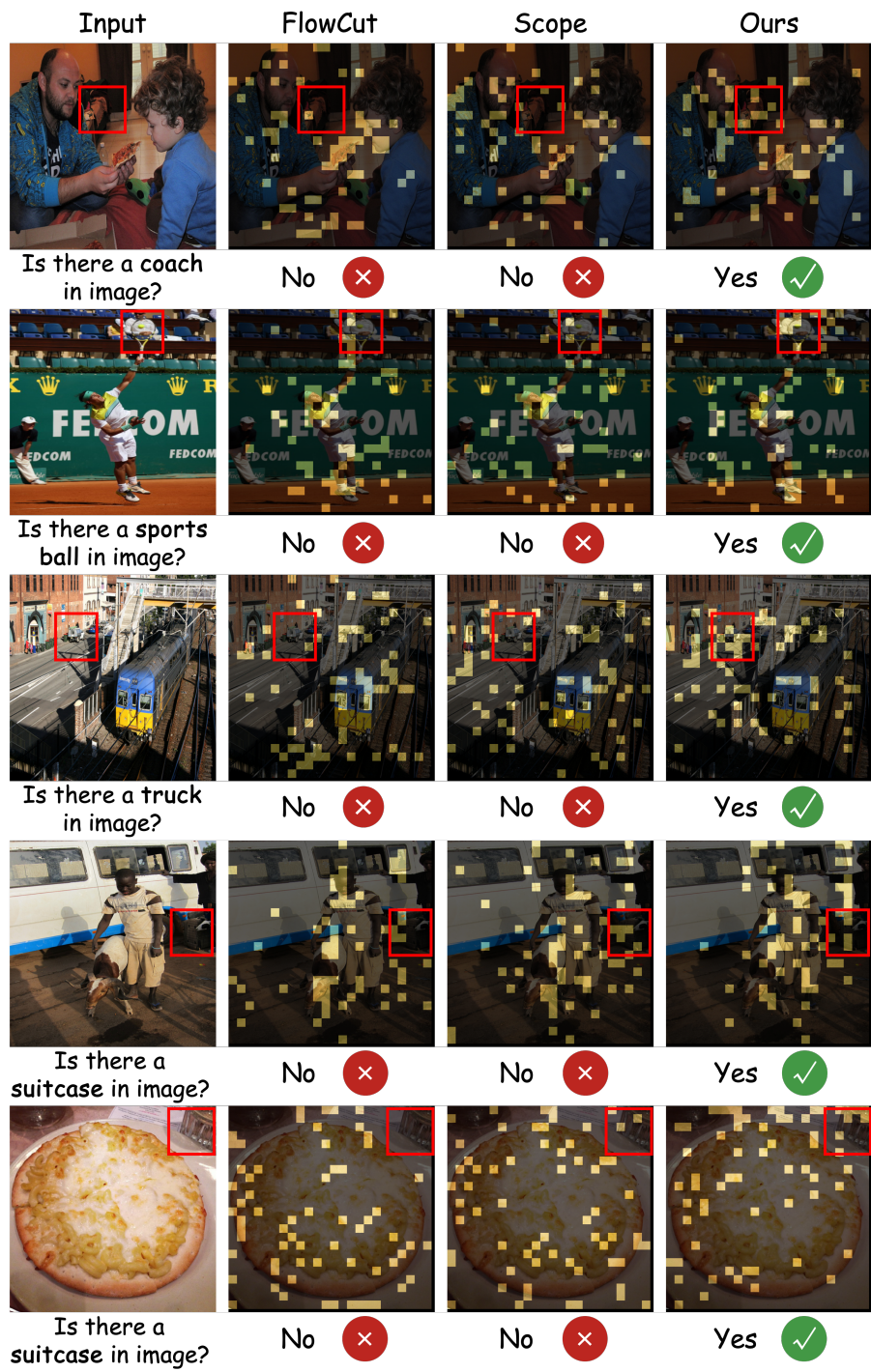


Figure 4: Qualitative visualization of selected visual tokens under a token budget of 64 on LLaVA-1.5-7B.